Electronic supplementary information (ESI†)

Opto-Mechano-Thermo-Sensitive Allochroic Luminescence Based on Coupled Dual Activators in Tantalate towards Multidimensional Stimulus Sensing

Rui Hu[a,b,c], Ying Zhang[d], Yan Zhao[a], Xusheng Wang[a*], Guorong Li[b*] and Mingxue Deng[b,c]

a. *Key Laboratory of Advanced Civil Engineering Materials of the Ministry of Education, Functional Materials Research Laboratory, School of Materials Science and Engineering, Tongji University, Shanghai 201804, China*

b. *Key Laboratory of Inorganic Functional Material and Device, Shanghai Institute of Ceramics, Chinese Academy of Sciences, Shanghai 200080, China*

c. *University of Chinese Academy of Sciences, Beijing 100049, China*

d. *Shanghai Institute of Microsystem and Information Technology, Chinese Academy of Sciences, Shanghai 200050, China*

[*] *Corresponding authors:*

E-mail: xs-wang@tongji.edu.cn (X. W.).

E-mail: grli@sunm.shcnc.ac.cn (G. L.).

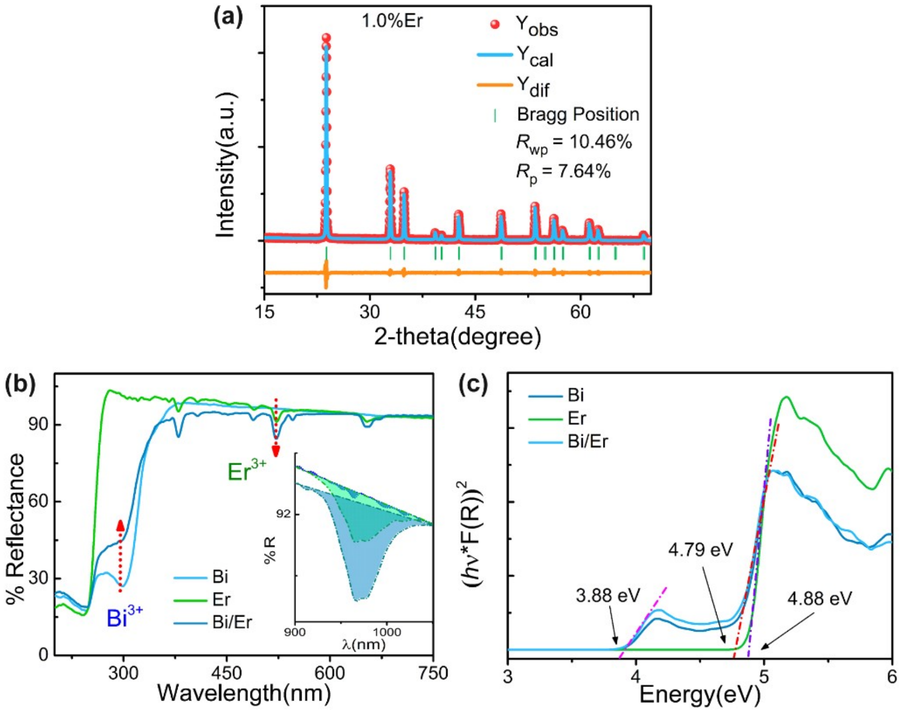

Fig. S1. (a) XRD pattern and Rietveld refinement of $LiTaO_3$:1.0%Er^{3+} sample. (b) Reflection spectra and (c) Kubelka−Munk plots with extrapolation of the bandgaps for $LiTaO_3$:1.0%Bi^{3+}, $LiTaO_3$:1.0%Er^{3+}, and $LiTaO_3$:1.0%Bi^{3+}/1.0%Er^{3+} phosphor.

Table S1. Exemplary refinement results for $LiTaO_3$:1.0%Er^{3+} and $LiTaO_3$:1.0%Bi^{3+}/0.7%Er^{3+} phosphor powder.

	1.0% Er^{3+}	1.0%Bi^{3+}/0.7%Er^{3+}
Space	*R*3*c*	*R*3*c*
a (Å)	5.1517	5.1552
c (Å)	13.7641	13.7768
c/a	2.6718	2.6724
V (Å^3)	316.352	317.085
Z	6	6

The diffuse reflectance spectra of $LiTaO_3$:1.0%Bi^{3+}, $LiTaO_3$:1.0%Er^{3+}, and $LiTaO_3$:1.0%Bi^{3+}/1.0%Er^{3+} phosphor are shown in Fig. S1b. The spectra exhibit intense absorption band ranging from 200 to 280 nm corresponding to the matrix absorption. Bi^{3+}

dopants produce an intense absorption band in the range of 280 to 380 nm, which is attributed to the $^1S_0 \rightarrow {}^3P_1$ transition of Bi^{3+}. Meanwhile, Er^{3+} codopants induce emerging peaks at 380 nm, 525 nm, 655 nm, and 980 nm, which are ascribed to the electron transitions from ground state to $^4G_{11/2}$, $^2H_{11/2}/^4S_{3/2}$, $^4F_{9/2}$, and $^4I_{11/2}$, respectively. When codoped with Bi^{3+} ions, Er^{3+} ions obtain enhanced characteristic absorption peaks, while the absorption intensity of Bi^{3+} declines along with the introduction of Er^{3+} ions. The experimental bandgap can be deduced from our diffuse reflectance spectra (DRS) using the Kubelka-Munk representation, which can define as $F(R) = \frac{(1-R)^2}{2R} = K/S$, where $F(R_\infty)$ represents the Kubelka-Munk function, R, K, and S are reflection, absorption, and scattering parameter, respectively.[1] For bandgap determination, Tauc plots $(F(R)hv)^2\ vs\ hv$ were employed as shown in Fig. S1c. The bandgap energy of both Bi^{3+}-doped and Bi^{3+}/Er^{3+}-codoped samples was calculated ~4.79 eV from the extrapolation of line for $(F(R)hv)^2 = 0$, which is slightly low compared with that of Er^{3+}-doped $LiTaO_3$ phosphor. Meanwhile, the energy of absorption edge was decreased to 3.88 eV by Bi^{3+} dopants.

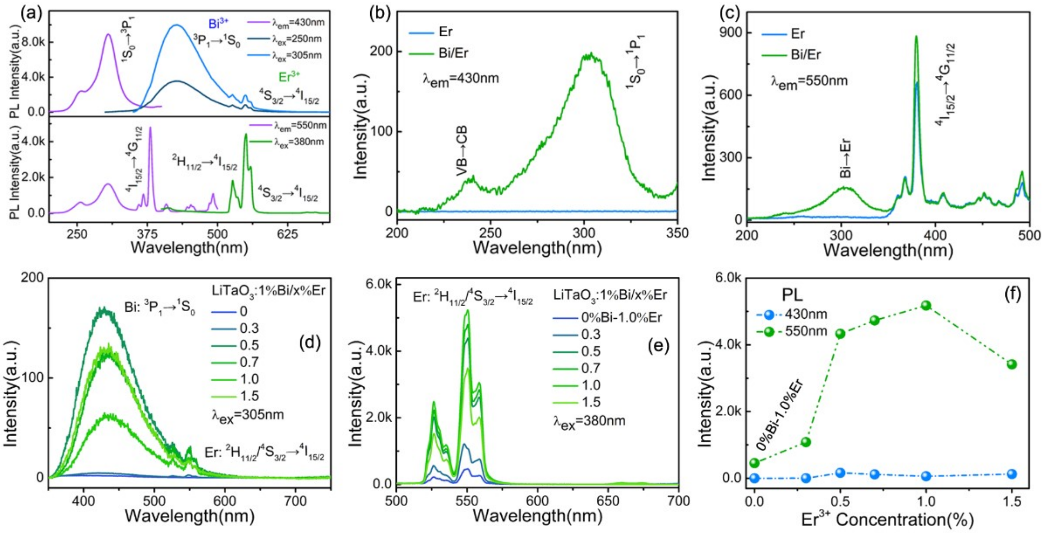

Fig. S2. (a) PL excitation and emission spectra of LiTaO$_3$:1.0%Bi^{3+}/1.0%Er^{3+} phosphor. Comparison of PL excitation spectra between LiTaO$_3$:1.0%Er^{3+} and LiTaO$_3$:1.0%Bi^{3+}/1.0%Er^{3+} monitoring at (b) 430 nm and (c) 550 nm respectively. Down-conversion emission spectra of LiTaO$_3$:1.0%Bi^{3+}/x%Er^{3+} (x = 0, 0.3, 0.5, 0.7, 1.0, and 1.5) under (d) 305 nm and (e) 380 nm excitation. (f) Concentration dependences of PL emission intensity at 430 nm (λ_{ex} = 305 nm) and 550 nm (λ_{ex} = 380 nm).

As for LiTaO$_3$:Bi^{3+}/Er^{3+} sample, both the characteristic emission of Bi^{3+} and Er^{3+} (peaking at ~430 nm and 550 nm respectively) have two excitation bands located at ~250 nm and 305 nm as shown in Fig. S2a. Besides the broad excitation bands, there is also a sharp excitation peak of Er^{3+} emission (Er^{3+}: $^4I_{15/2} \rightarrow {}^4G_{11/2}$ transition, peaking at 380 nm) in PL excitation spectrum of LiTaO$_3$:Bi^{3+}/Er^{3+}. As shown in Fig. S2b, the excitation band of Bi^{3+} at ~250 nm is attributed to the charge transfer band of host, meanwhile the stronger band at ~305 nm originates from $^1S_0 \rightarrow {}^3P_1$ transition. Compared with Er^{3+}-doped LiTaO$_3$ sample, Bi^{3+} dopants introduce new excitation bands for the characteristic emission of Er^{3+} in the range of 200-350 nm. It proves that there is efficient energy transfer from Bi^{3+} to Er^{3+} ions resulting in noticeable down-conversion PL of Er^{3+} ions, when LiTaO$_3$:Bi^{3+}/Er^{3+} is under UV irradiation. Upon 305 nm excitation, the PL spectrum of LiTaO$_3$:Bi^{3+}/Er^{3+} extends from 350 to 600 nm centered at 430 nm. Specially, there is also significant emission peaks owing to

$^2H_{11/2}/^4S_{3/2} \rightarrow {}^4I_{15/2}$ transitions of Er^{3+} in PL spectra, which overlap with broad band of Bi^{3+} emitters ($^3P_1 \rightarrow {}^1S_0$). Nevertheless, the emission curve generated by 380 nm excitation only shows single-region peaks at 525 nm and 550 nm appearing in green. Furthermore, when the Er^{3+} content is below 1.0%, PL intensity elevates with the augment of x value under 305 nm and 380 nm excitation. Afterward, the intensity begins to weaken along with the increment of Er^{3+} ions, which can be attributed to concentration quenching effect

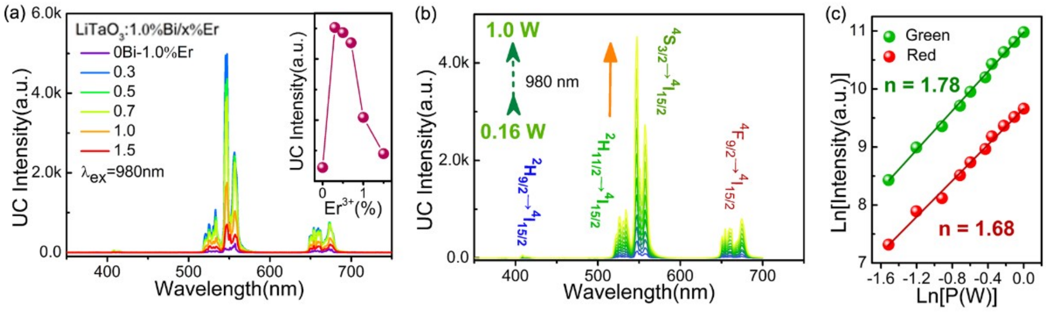

Fig. S3. (a) UC PL emission spectra of $LiTaO_3$:1.0%Er^{3+} and $LiTaO_3$:1.0%Bi^{3+}/x%Er^{3+} (x = 0.3, 0.5, 0.7, 1.0, and 1.5) under 980 nm excitation. Inset is concentration dependence of emission intensity. (b) Dependence of the UC PL spectra on the 980 nm laser power. (c) Intensity dependence of green and red emission bands ($^2H_{11/2}/^4S_{3/2} \rightarrow {}^4I_{15/2}$ and $^4F_{9/2} \rightarrow {}^4I_{15/2}$ transitions of Er^{3+}) on the laser power.

In contrast to down-conversion emission performance, the up-conversion emission of $LiTaO_3$:Bi^{3+}/Er^{3+} is more sensitive to Er^{3+} content. Bi^{3+} ions can significantly improve the UC PL intensity of Er^{3+} ions, but samples with low Er^{3+} codoping content show more increment in intensity. In addition, its UC PL spectra have another two peaks located at 410 nm and 670 nm respectively, which are attributed to $^2H_{9/2} \rightarrow {}^4I_{15/2}$, $^4F_{9/2} \rightarrow {}^4I_{15/2}$ transition respectively.[2] The power dependent UC PL spectra suggest that the intensity has a positive correlation with excitation power. The n values which were calculated from logarithmic dependence power versus emitting intensity, prove that two-photon process contributes to green and red UC PL emission.[3]

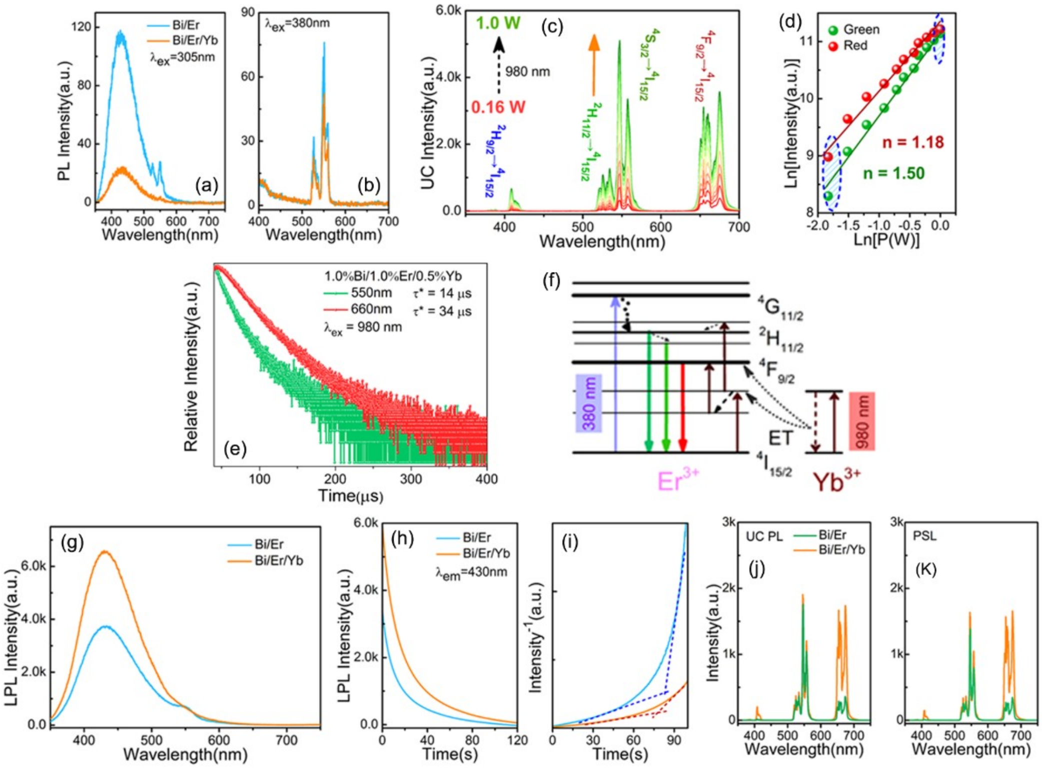

Fig. S4. PL, long-persistent, and photostimulated emission performance of $LiTaO_3$:1.0%Bi^{3+}/1.0%Er^{3+}/0.5%Yb^{3+}. (a)-(b) Down-conversion emission spectra of $LiTaO_3$:1.0%Bi^{3+}/1.0%Er^{3+} and $LiTaO_3$:1.0%Bi^{3+}/1.0%Er^{3+}/0.5%Yb^{3+} under 305 nm and 380 nm excitation respectively. (c) Dependence of the UC PL spectra of $LiTaO_3$:Bi^{3+}/Er^{3+}/Yb^{3+} on the 980 nm laser power, and (d) the emission intensity dependence on the laser power. (e) UC PL decay profiles at 550 nm and 660 nm upon 980 nm excitation. (f) Mechanism of multimode PL emission in diverse color for $LiTaO_3$:Bi^{3+}/Er^{3+}/Yb^{3+}. (g) Afterglow spectra of pre-irradiated $LiTaO_3$:Bi^{3+}/Er^{3+}, $LiTaO_3$:Bi^{3+}/Er^{3+}/Yb^{3+}. (h) Afterglow decay curves of pre-irradiated $LiTaO_3$:Bi^{3+}/Er^{3+}, $LiTaO_3$:Bi^{3+}/Er^{3+}/Yb^{3+}, and (i) the relationship of reciprocal afterglow intensity versus time. (j) UC PL and (k) PSL emission spectra of $LiTaO_3$:Bi^{3+}/Er^{3+}, $LiTaO_3$:Bi^{3+}/Er^{3+}/Yb^{3+} sample upon 980 nm laser irradiation.

Yb^{3+} codopants obviously decrease the down-conversion emission intensity of Bi^{3+} and Er^{3+} ions in $LiTaO_3$ host, but can enhance the UC PL of Er^{3+} ions under 980 nm excitation. The negative effect of Yb^{3+} on down-conversion performance originates from the increasing trap density which can capture and store excited electrons leading to less radiative recombination of excited electrons and activators.[4] Meanwhile, due to the energy transfer effect from Yb^{3+} to Er^{3+} ions, the UC PL intensity of sample enhances obviously. On the other hand, Yb^{3+} ions also improve the red emission in up-conversion emission process significantly, resulting in higher intensity ratio of red and green emission. When the pump power improves, the intensity ratio of red and green declines slightly, but all emissions are still attributed to two-photon process. All up-conversion emission lifetimes of Er^{3+} ions decline by half with introducing Yb^{3+} ions. Thus, the down-conversion PL mechanism of $LiTaO_3:Bi^{3+}/Er^{3+}/Yb^{3+}$ is similar to that of $LiTaO_3:Bi^{3+}/Er^{3+}$, while Yb^{3+} ions can increase red emission intensity of UC PL by enriching the population of $^4F_{9/2}$ level via a suitable energy transfer (ET) process.[5] Because of the increasing trap density induced by Yb^{3+} codopants, the afterglow intensity, afterglow lifetime, and PSL intensity show an apparent increment. The nonlinear dependence of reciprocal intensity versus decay time indicates that the trap depth of $LiTaO_3:Bi^{3+}/Er^{3+}/Yb^{3+}$ is also not in continuous distribution, and the long-persistent emission originates from two or more effective trap centers.

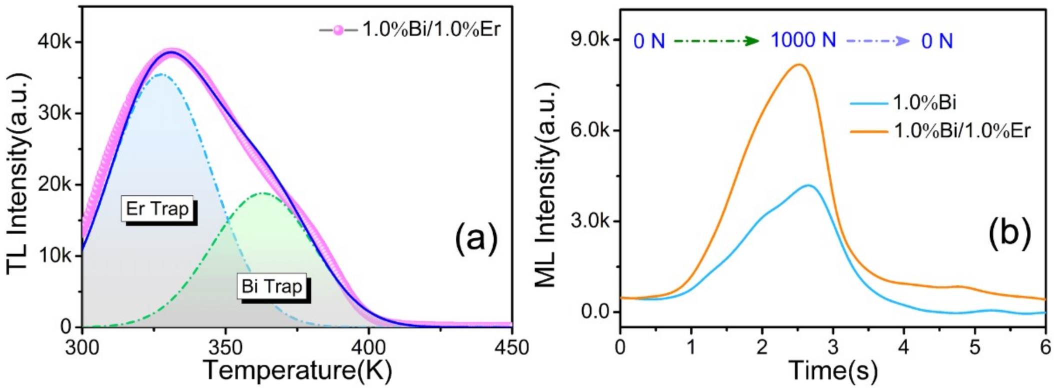

Fig. S5. (a) The fitted results of TL glow curve for pre-irradiated $LiTaO_3$:1.0%Bi^{3+}/1.0%Er^{3+}. (b) The ML intensity curves of various samples under gradually changing load.

Table S2. TL parameters of $LiTaO_3$:1.0%Bi^{3+}/1.0%Er^{3+}.

Trap	T_A(K)	T_m(K)	T_B(K)	τ	δ	ω	μ_g	E(eV)
T_{Er}	306	327	348	22	20	42	0.486	0.643
T_{Bi}	343	363	384	20	21	41	0.510	0.894

In order to investigate the effect of different traps on ML, LPL, and PSL property, the TL curve of $LiTaO_3$:1.0%Bi^{3+}/1.0%Er^{3+} was decomposed into several peaks. Then a classical fitting peak shape method developed by Chen[6] was introduced, the trap depths (*E*) were calculated from the glow-peak parameters according to the following equation:

$$E = [2.52 + 10.2(\mu g - 0.42)]\frac{\kappa B T_m^2}{\omega} - 2\kappa B T_m$$

(1)

where μ_g is symmetry factor, T_m is the maximum value of peak temperature and T_1, T_2 are the temperature on either side of TL peak at half height respectively, κ is Boltzmann's constant. $\mu_g = \delta/\omega$ is the symmetrical geometrical factor, $\delta = T_2 - T_m$ is the half-width toward the falloff of the glow peak, $\omega = \delta + \tau$ is the total half-width, and□ τ□is the half-width at the low-temperature side of TL peak, which can be obtained by formula calculation ($\tau = T_m - T_1$). The trap depths of T_{Er} and T_{Bi} traps are calculated as 0.643 eV, 0.894 eV, respectively.

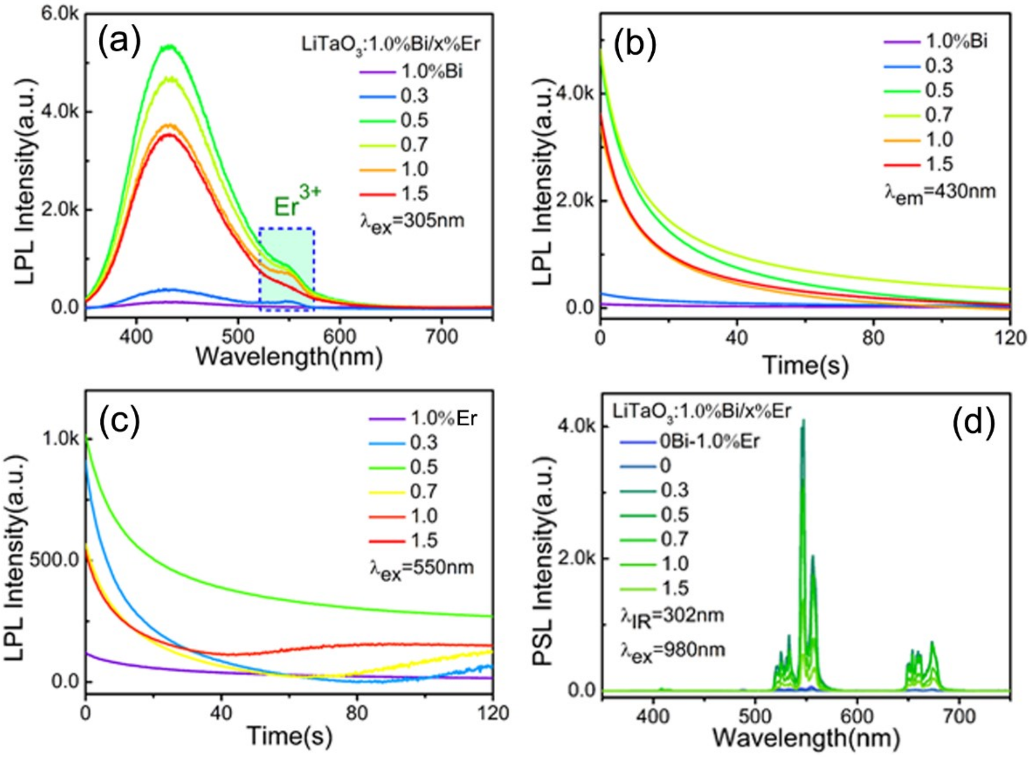

Fig. S6. (a) Afterglow spectra of LiTaO$_3$:1.0%Bi^{3+}/x%Er^{3+} (x = 0, 0.3, 0.5, 0.7, 1.0, and 1.5) after 305 nm irradiation for 3 min. (b)-(c) LPL decay curves monitored at 430 nm and 550 nm. (d) PSL emission spectra of LiTaO$_3$:1.0%Bi^{3+}/x%Er^{3+} (x = 0, 0.3, 0.5, 0.7, 1.0, and 1.5) and LiTaO$_3$:1.0%Er^{3+} upon 980 nm stimulation.

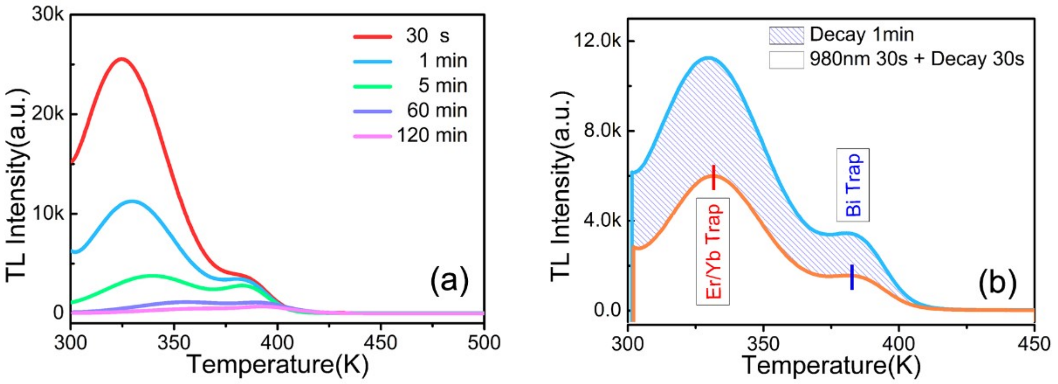

Fig. S7. (a) TL glow curves of pre-irradiated $LiTaO_3$:1.0%Bi^{3+}/1.0%Er^{3+}/0.5%Yb^{3+} after decay for a period of time. (b) TL glow curves of $LiTaO_3$:1.0%Bi^{3+}/1.0%Er^{3+}/0.5%Yb^{3+} after decay in the dark (1 min) or 980 nm stimulation (photo-stimulation for 30 s then decay for 30 s).

Yb^{3+} codopants improve the density of shallow traps in $LiTaO_3$ host obviously, thus the initial LPL intensity of $LiTaO_3$:Bi^{3+}/Er^{3+}/Yb^{3+} gains a significant enhancement. However, the decay rate of LPL emission is enhanced due to the worse resistance of shallow traps to thermal agitation. Whereas, Yb^{3+} ions improve the durability of charge carriers in overall traps under NIR stimulation, thus charge carriers in traps can be released at a slower rate via photo-stimulation.

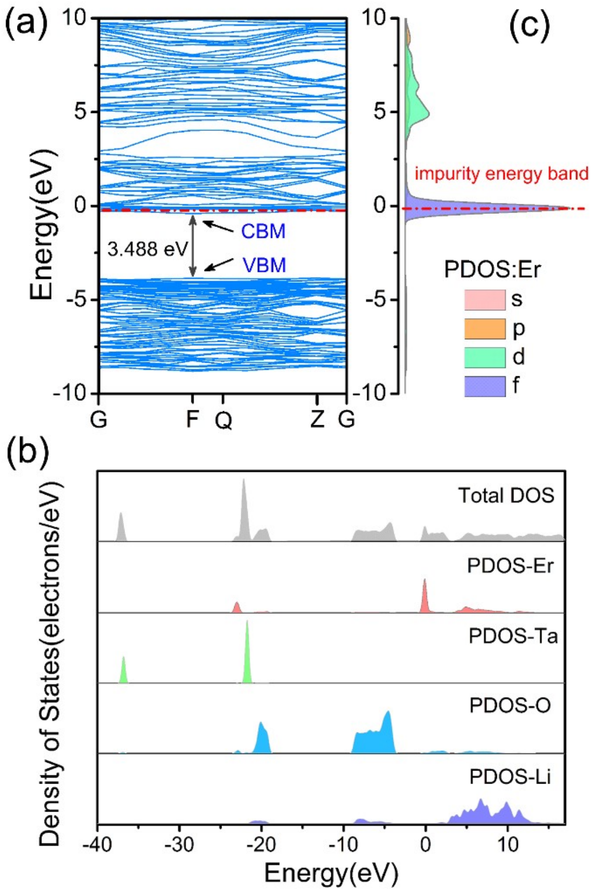

Fig. S8. (a) Band structures of $LiTaO_3:Er^{3+}$; (b) total and partial density of states of $LiTaO_3:Er^{3+}$; (c) partial density of states of Er codopants.

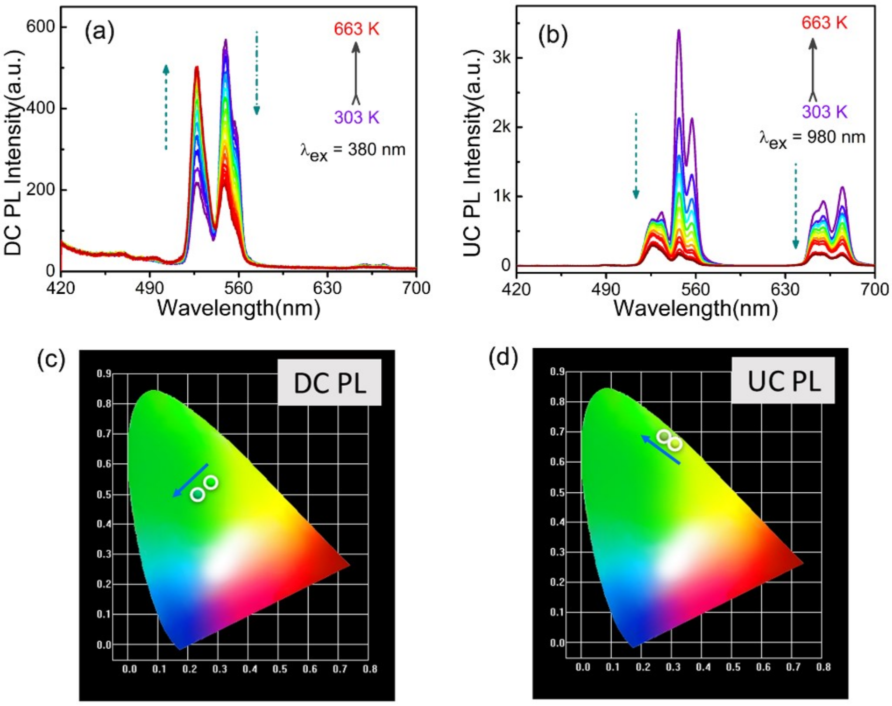

Fig. S9. Temperature dependent down- (a) and up-conversion (b) PL emission spectra of $LiTaO_3$:1.0%Bi^{3+}/1.0%Er^{3+} in the temperature range of 303-663 K, and (c)-(d) the relevant CIE chromaticity coordinates.

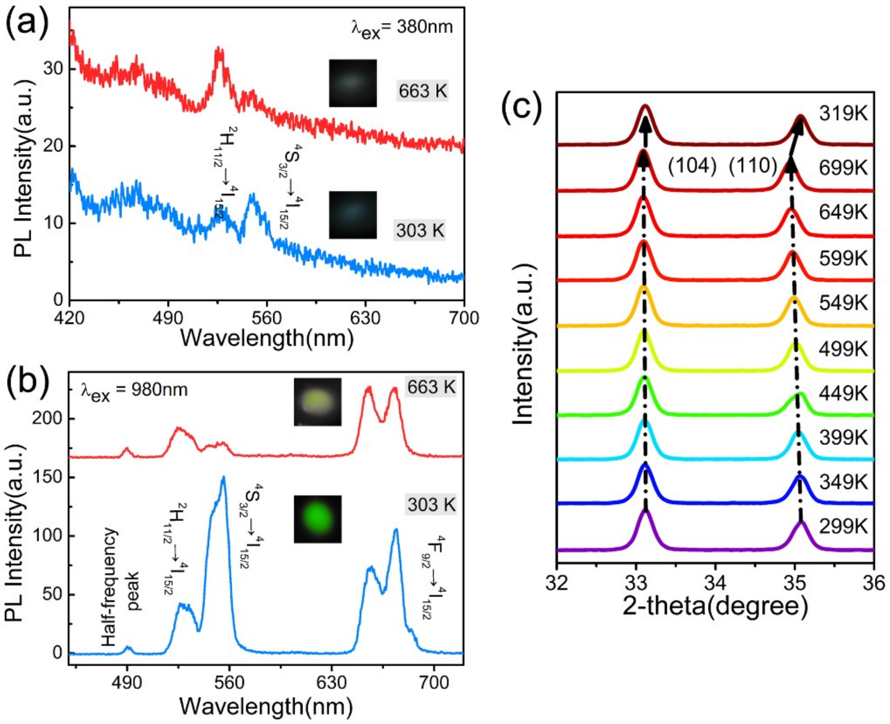

Fig. S10. (a) Down-conversion emission (λ_{ex} = 380 nm) and (b) up-conversion emission (λ_{ex} = 980 nm) spectra of $LiTaO_3$:1.0%Er^{3+} at 303 K and 663 K. (c) Temperature dependent XRD patterns of $LiTaO_3$:1.0%Er^{3+} powder.

References

[1] H. Li, R. Pang, G. Liu, W. Sun, D. Li, L. Jiang, S. Zhang, C. Li, J. Feng, H. Zhang, Synthesis and Luminescence Properties of Bi^{3+}-Activated K_2MgGeO_4: A Promising High-Brightness Orange-Emitting Phosphor for WLEDs Conversion. *Inorg. Chem.* 2018, 57, 12303-12311.

[2] A. Pandey, V. K. Rai, V. Kumar, V. Kumar, H. C. Swart, Upconversion Based Temperature Sensing Ability of Er^{3+}-Yb^{3+}Codoped $SrWO_4$:An Optical Heating Phosphor. *Sensors and Actuators B: Chemical* 2015, **209**, 352-358.

[3] Y. Li, Z. Song, C. Li, R. Wan, J. Qiu, Z. Yang, Z. Yin, Y. Yang, D. Zhou, Q. Wang, High Multi-photon Visible Upconversion Emissions of Er^{3+} Singly Doped BiOCl Microcrystals: A Photon Avalanche of Er^{3+} Induced by 980 nm Excitation. *Appl. Phys. Lett.* 2013, **103**, 231104.

[4] J. Ueda, S. Miyano, S. Tanabe, Formation of Deep Electron Traps by Yb^{3+} Codoping Leads to Super-Long Persistent Luminescence in Ce^{3+}-Doped Yttrium Aluminum Gallium Garnet Phosphors. *ACS Appl. Mater. Inter.* 2018, **10**, 20652-20660.

[5] Q. Zhang, S. Yue, H. Sun, X. Wang, X. Hao, S. An, Nondestructive Up-conversion Readout in Er/Yb Co-doped $Na_{0.5}Bi_{2.5}Nb_2O_9$-Based Optical Storage Materials for Optical Data Storage Device Applications. *J. Mater. Chem. C* 2017, **5**, 3838-3847.

[6] R. Chen, Glow Curves with General Order Kinetics. *J. Electrochem. Soc.* 1969, **116**, 1254-1257.